Dalton Transactions

ROYAL SOCIETY OF CHEMISTRY

PAPER

View Article Online
View Journal | View Issue

Cite this: *Dalton Trans.*, 2021, **50**, 16326

Influence of temperature on the equilibria of oxidovanadium(IV) complexes in solution†

Daniele Sanna, [a] Giuseppe Lubinu,[b] Valeria Ugone *[a] and Eugenio Garribba [b]

Received 11th August 2021,
Accepted 17th October 2021

DOI: 10.1039/d1dt02680a

rsc.li/dalton

The equilibria in the solution of three different oxidovanadium(IV) complexes, $VO(dhp)_2$ (dhp = 1,2-dimethyl-3-hydroxy-4(1*H*)-pyridinonato), $VO(ma)_2$ (ma = maltolato) and $VO(pic)_2(H_2O)$ (pic = picolinato), were examined in the temperature range of 120–352 K through a combination of instrumental (EPR spectroscopy) and computational techniques (DFT methods). The results revealed that a general equilibrium exists: $VOL_2 + H_2O \rightleftarrows$ *cis*-$VOL_2(H_2O) \rightleftarrows$ *trans*-$VOL_2(H_2O)$, where *cis* and *trans* refer to the relative position of H_2O and the oxido ligand. The equilibrium is more or less shifted to the right depending on the ligand, the temperature, the ionic strength and the coordinating properties of the solvent. With $VO(dhp)_2$, only the square pyramidal species exists at 298 K in aqueous solution, while at 120 K the *cis*- and *trans*-$VO(dhp)_2(H_2O)$ species are also present. The complex of maltol exists almost exclusively in the form *cis*-$VO(ma)_2(H_2O)$ in aqueous solution at 298 K, while the *trans* species can be revealed only at higher temperatures, where the EPR linewidth significantly decreases. The equilibria involving 1-methylimidazole (MeIm), a model for the side chain His coordination, are also influenced by temperature, with its coordination being favored by decreasing the temperature. The implications of these results in the study of the (vanadium complex)–protein systems are discussed and the interaction with myoglobin (Mb) is examined as a representative example.

1. Introduction

Vanadium compounds have been shown to be a new class of potential metallodrugs due to their promising pharmacological properties as antidiabetic, antitumoral and antiviral drugs.[1–10]

The main problem with orally administered V compounds is their poor absorption in the gastrointestinal tract.[11,12] To overcome this limitation, neutral $V^{IV}OL_2$ complexes were proposed and the benchmark compound for these studies is VO(ma)$_2$, bis(maltolato)oxidovanadium(IV) or BMOV.[13,14]

After absorption in the gastrointestinal tract, $V^{IV}OL_2$ complexes reach the bloodstream where they encounter high and low molecular mass components. Therefore, the vanadium–protein interaction has been intensively studied for several years in order to understand their role in metal transport.[15–31] Several instrumental tools have been applied to study the binding of $V^{IV}OL_2$–protein, such as X-ray diffraction analysis, UV-Vis spectroscopy, circular dichroism, mass spectrometry, ENDOR and ESEEM, but surely Electron Paramagnetic Resonance (EPR) spectroscopy is one of the most used techniques to characterize the interaction of V^{IV} species with biomolecules.[32] Usually, EPR spectra are recorded at low temperatures (77 or 120 K) since anisotropic spectra allow one to get information on the symmetry and the coordination geometry of the $V^{IV}O$ complexes, the identity of the equatorial ligands through the A_z value (more sensitive to the equatorial donors than isotropic A_0), and the presence of minor species in solution.[32,33] In contrast, EPR spectra are often little informative at 298 K because the lines are not narrow enough to allow for distinguishing the presence of more than one species in solution with similar A_0 values. However, spectra recorded at 298 K can give some important information about the V–protein interaction; indeed, an anisotropic spectrum is expected when the binding is strong enough to block the metal species on the protein surface (hindering the rotational motion in the EPR time scale), while an isotropic spectrum is expected when the complexes are free to rotate in solution and no covalent binding or weak non-covalent interaction occurs.[32]

During the last few years, EPR spectroscopy allowed for demonstrating that the interaction with proteins depends on the thermodynamic stability and geometry assumed by $V^{IV}OL_2$ complexes in aqueous solution.[32] In fact, a non-covalent interaction or a weak axial binding is expected for stable $V^{IV}OL_2$ complexes,[15,34] an equatorial binding for *cis*-octahedral $V^{IV}OL_2(H_2O)$ species after the replacement of the water mole-

[a]*Istituto di Chimica Biomolecolare, Consiglio Nazionale delle Ricerche, Trav. La Crucca 3, I-07100 Sassari, Italy. E-mail: valeria.ugone@cnr.it*
[b]*Dipartimento di Chimica e Farmacia, Università di Sassari, Via Vienna 2, I-07100 Sassari, Italy*

†Electronic supplementary information (ESI) available. See DOI: 10.1039/d1dt02680a

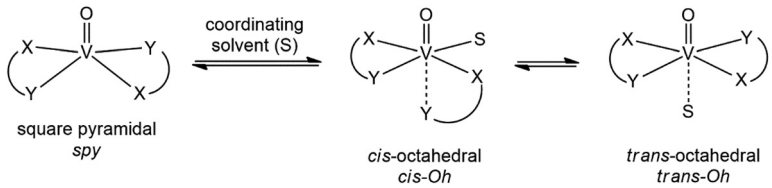

Scheme 1 Equilibrium between the square pyramidal, *cis*- and *trans*-octahedral species, where *cis* and *trans* refer to the relative positions of solvent S (H_2O in aqueous solution) and the oxido ligand. In the text, they are denoted with *spy*, *cis-Oh*, and *trans-Oh*, respectively.

cule with an amino acid side-chain,[15,18,35,36] and the interaction with two adjacent positions of the moiety $V^{IV}OL^{+}$ for bis-chelated complexes with low stability.[25–27]

Depending on the ligand, the equilibria shown in Scheme 1 are possible for a $V^{IV}OL_2$ complex.[37–39] It has been already shown that these equilibria can be affected by temperature[40] and this should be considered when the spectral data are collected at low temperatures. In other words, the type of interaction and the composition and structure of the adducts could depend on the temperature.

In this study, the influence of temperature on the solution equilibria of oxidovanadium(IV) complexes was studied. In particular, $VO(dhp)_2$ (dhp = 1,2-dimethyl-3-hydroxy-4(1*H*)-pyridinonato), $VO(ma)_2$ (ma = maltolato) and $VO(pic)_2(H_2O)$ (pic = picolinato) were examined in the temperature range of 120–352 K through a combination of instrumental (EPR spectroscopy) and computational techniques (DFT methods). The results were applied to the analysis of the systems formed by $V^{IV}OL_2$ and myoglobin (Mb).

2. Experimental and computational section

2.1. Chemicals

Water was deionized prior to use through a Millipore Milli-Q Academic purification system. Methanol, chloroform, and toluene were purchased from Sigma-Aldrich. The chemicals oxidovanadium(IV) sulfate trihydrate ($VOSO_4{\cdot}3H_2O$), pyridine-2-carboxylic acid (picolinic acid), 3-hydroxy-2-methyl-4*H*-pyran-4-one (maltol), 1,2-dimethyl-3-hydroxy-4(1*H*)-pyridinone (deferiprone), 1-methylimidazole (MeIm), myoglobin from equine heart (Mb, M1882) and 4-(2-hydroxyethyl)-piperazine-1-ethanesulfonic acid (HEPES) were Sigma-Aldrich products of the highest grade available and used as received.

The complexes $[V^{IV}O(dhp)_2]$, $[V^{IV}O(ma)_2]$ and $[V^{IV}O(pic)_2(H_2O)]$ were synthesized following the procedure established in the literature.[41–43] $[VO(dhp)_2]$: yield 86%; C, 48.79; H, 4.94; N, 7.96 (calc. for $C_{14}H_{16}N_2O_5V$: C, 48.99; H, 4.70; N, 8.16); ESI-MS(+), $[VO(dhp)_2 + H]^+$ 344.06 *m/z.* $[VO(ma)_2]$: yield 88%; C, 45.45; H 3.18 (calc. for $C_{12}H_{10}O_7V$: C, 45.47; H, 3.16); ESI-MS(+), $[VO(ma)_2 + H]^+$ 317.99 *m/z.* $[VO(pic)_2(H_2O)]$: yield 60%; C, 43.72; H, 3.18; N, 8.42 (calc. for $C_{12}H_{10}N_2O_6V$, 43.79; H, 3.06; N, 8.51); ESI-MS(+), $[VO(pic)_2 + H]^+$ 311.99 *m/z*; ESI-MS(−), $[VO(pic)_2(OH)]^-$ 326.98 *m/z*.

2.2. Analytical and spectroscopic measurements

Elemental analysis (C, H, and N) was carried out using a PerkinElmer 240 B elemental analyser. ESI-MS spectra were recorded using a high-resolution Q Exactive™ Plus Hybrid Quadrupole-Orbitrap™ mass spectrometer (Thermo Fisher Scientific). The solutions, obtained by dissolving the solid compounds in LC-MS H_2O (V concentration 5×10^{-6} M), were infused at a flow rate of 5.00 μL min^{-1} into the ESI chamber. The spectra were recorded in the range of *m/z* 50–750 with a resolution of 140 000. The instrumental conditions for the ESI-MS(+) measurements were: a spray voltage of 2300 V, a capillary temperature of 250 °C, sheath gas 5 (arbitrary units), auxiliary gas 3 (arbitrary units), sweep gas 0 (arbitrary units), and a probe heater temperature of 50 °C. The instrumental conditions for the ESI-MS(−) measurements were: a spray voltage of −1900 V, a capillary temperature of 250 °C, sheath gas 20 (arbitrary units), auxiliary gas 5 (arbitrary units), sweep gas 0 (arbitrary units), and a probe heater temperature of 14 °C. The mass spectra were analysed by using the Thermo Xcalibur 3.0.63 software (Thermo Fisher Scientific).

The aqueous solutions for EPR measurements were prepared by dissolving $VOSO_4{\cdot}3H_2O$ and the ligand (L = ma, dhp, and pic) in ultrapure water to get a $V^{IV}O^{2+}$ concentration of 1.0×10^{-3} M and a metal-to-ligand molar ratio of 1/2. HEPES buffer of 0.1 M concentration was added and the pH value was adjusted to the desired value. In the ternary systems, an appropriate amount of Mb or MeIm was added to the V–L solutions to obtain a $V^{IV}O^{2+}$/L/Mb molar ratio of 1/2/1 or $V^{IV}O^{2+}$/L/MeIm 1/2/4, respectively.

The solutions prepared in the absence of the HEPES buffer were obtained by dissolving an appropriate amount of the solid compound in the solvent or solvent mixture ($CHCl_3$/toluene 6/4 v/v, MeOH or H_2O/MeOH 9/1 v/v) to obtain a concentration of 1.0×10^{-3} M.

Argon was bubbled through all the solutions to ensure the absence of oxygen and avoid the oxidation of $V^{IV}O^{2+}$ ions.

For frozen solution EPR measurements, DMSO is usually added to the aqueous samples to get a better resolution of the spectra. However, as the addition of this solvent can influence the equilibria in solution and denature the proteins, HEPES was used for EPR measurements at 120 K, which allowed us to achieve a good resolution of the spectra.

HEPES solutions were also used for measurements at 298 K or higher temperatures in order to have the same solvent composition at different temperatures. The use of a buffer instead

of organic solvents is a good strategy to have more significant results from a biological point of view and can be extended to different proteins.

The EPR spectra were recorded using an X-band Bruker EMX spectrometer equipped with an HP 53150A microwave frequency counter. The instrumental parameters were as follows: microwave frequency, 9.40–9.41 GHz at 120 K and 9.83–9.84 GHz at 298–352 K; microwave power, 20 mW; time constant, 81.92 ms; modulation frequency, 100 kHz; modulation amplitude, 0.4 mT; and resolution, 4096 points. When the samples were transferred into the EPR tubes (120 K) or a Bruker AquaX cell (298 K), the spectra were immediately measured. Signal averaging was used to increase the signal-to-noise ratio.[44] The EPR spectra at variable temperatures (298–352 K) were measured in capillary tubes and the temperature was controlled using a variable temperature unit ER4131VT. The recorded spectra were simulated with the software Bruker WINEPR SimFonia (version 1.26 (beta), Bruker Analytik GmbH, 1997).

2.3. DFT calculations

DFT calculations were carried out with Gaussian 09 (revision C.01).[45] The $V^{IV}O$ complex geometries and their relative stability were computed at the level of theory B3P86/6-311g(d,p); this method guarantees a good degree of accuracy in the structural optimization of first-row transition metal complexes[46,47] and, particularly, of vanadium compounds.[48] Water was simulated within the framework of the SMD model.[49]

For dhp complexes, the relative stability of the bis-chelated species at 298 and 120 K was determined by calculating the value of ΔG_{aq} for the equilibrium in solution:

$$[VOL_2] + H_2O \rightleftharpoons \textit{cis}\text{-}[VOL_2(H_2O)] \quad (1)$$

All the different possible geometries of the square pyramidal and *cis*-octahedral isomers were considered (Scheme S1†).

In the case of ma and pic species, only the most stable *cis*-octahedral structures were considered in the DFT calculations (Schemes S2 and S3†), as suggested by previous studies[36] and references therein.

The Gibbs energy in aqueous solution (G_{aq}) for each species can be separated into the electronic plus nuclear repulsion energy (E_{ele}), the thermal contribution (G_{therm}) and the solvation energy (ΔG_{solv}): $G_{aq} = E_{ele} + G_{therm} + \Delta G_{solv}$. The term $RT\ln(24.46)$ was considered to account for the standard state correction from the gas phase to the aqueous solution. The thermal contribution was estimated using the ideal gas model and the calculated harmonic vibrational frequencies to determine the correction due to the zero-point energy and the thermal population of the vibrational levels.

The *trans-Oh* isomers were not considered as it was noticed that, using this level of calculation with the SMD model for water, they are distorted toward the *spy* species. Furthermore, experimental evidence suggests that these species are less stable than *cis-Oh*, being present in solution in small amounts.

For the evaluation of protein binding, the structures of the model complex $[VOL_2(MeIm)]$ (with L = ma, pic, and dhp) were computed by considering all the possible orientations of 1-methylimidazole. The latter has been used since it is a good model for histidine coordination.[15] A relaxed scan calculation was performed by changing the dihedral angle O=V–N_{MeIm}–C_{MeIm} from 0° to 360° (with the ligand parallel to V=O when the angle is 0 or 180° and perpendicular when the angle is 90 or 270°), with an increment of 10° in the case of dhp complexes. The structures of the most stable isomers, namely those corresponding to the minima E_{aq} (electronic energy in solution) in the scan calculation, were subsequently optimized and used in the calculation of thermodynamic parameters. The Gibbs energy in aqueous solution (ΔG_{aq}) was computed considering the following reactions:

$$[VOL_2] + Melm \rightleftharpoons \textit{cis}\text{-}[VOL_2(Melm)] \quad (2)$$

$$\textit{cis}\text{-}[VOL_2(H_2O)] + Melm \rightleftharpoons \textit{cis}\text{-}[VOL_2(Melm)] + H_2O \quad (3)$$

In the systems with ma and pic, instead of doing a scan calculation, the structures of *cis*-$[VOL_2(MeIm)]$ with dihedral angles θ = 0, 90, 180, and 270° were optimized. All the frequency calculations were done both at 298.15 K, the default temperature in Gaussian 09, and at 120 K.

The ΔG_{aq} values obtained from the DFT calculations are not necessarily coincident with the real values as they were calculated with the SMD model instead of using explicit solvent molecules; therefore, only the relative values at 298 and 120 K are relevant for the purposes of this study.

For the optimized structures of both binary and ternary species, the ^{51}V hyperfine coupling constants (A) were calculated using the half-and-half hybrid functional BHandHLYP and the basis set 6-311+g(d), according to the procedures previously published.[50–55] It must be taken into account that for a $V^{IV}O^{2+}$ species, A_z is usually negative; however, in the literature its absolute value is often reported and this formalism was also used in this study. The theoretical background is described in detail in ref. 56–58. The percent deviation (PD) of the absolute calculated value, A_z^{calcd}, from the absolute experimental value, A_z, was obtained as follows: $100 \times [(A_z^{calcd} - A_z)/A_z]$.

3. Results and discussion

3.1. Systems with dhp

The behavior of the $[VO(dhp)_2]$ complex in solution has been already studied by the pH-potentiometric, EPR and DFT methods.[39,41] The EPR spectra recorded at 120 K suggest that, in the pH range 5–8, the bis-chelated species is present in solution as a mixture of the square pyramidal $[VO(dhp)_2]$ and octahedral *cis*-$[VO(dhp)_2(H_2O)]$ in equilibrium between each other, together with a small amount of *trans*-$[VO(dhp)_2(H_2O)]$,[39] this latter species revealed when the spectra were recorded at 1 mM concentration.

In the present study, the results at low temperatures were reanalyzed and it was confirmed that the resonances of the third species with lower A_z (which corresponds to *trans*-[VO $(dhp)_2(H_2O)$] where the water molecule is coordinated in the

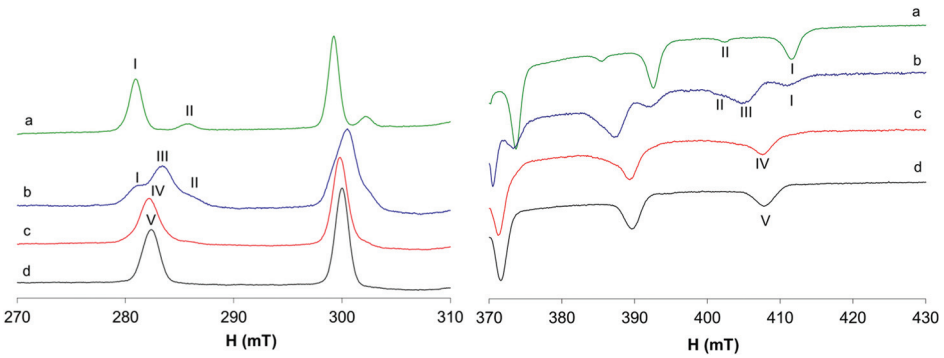

Fig. 1 Anisotropic EPR spectra recorded at 120 K in frozen solutions containing: (a) solid $VO(dhp)_2$ 1 mM dissolved in a mixture H_2O/MeOH 9/1; (b) VO^{2+}/dhp 1/2, VO^{2+} 1 mM, HEPES 0.1 M, pH 7.40; (c) VO^{2+}/dhp/Mb 1/2/1, VO^{2+} 1 mM, HEPES 0.1 M, pH 7.40; and (d) VO^{2+}/dhp /MeIm 1/2/4, VO^{2+} 1 mM, HEPES 0.1 M, pH 7.40. With **I**, **II**, **III**, **IV** and **V** the parallel resonances of *cis*-[$VO(dhp)_2(H_2O)$], *trans*-[$VO(dhp)_2(H_2O)$], [$VO(dhp)_2$], *cis*-$VO(dhp)_2$(Mb) and [$VO(dhp)_2$(MeIm)] are indicated.

axial position) are present when the spectrum is recorded in HEPES buffer (0.1 M) at physiological pH (Fig. 1b, **II**). To evaluate if the buffer and other ions (as SO_4^{2-} from $VOSO_4$ salt) can influence the equilibrium between the species in solution, the spectrum was recorded by dissolving the solid complex $VO(dhp)_2$ in a mixture H_2O/MeOH 9/1 v/v (Fig. 1a). At these experimental conditions, the predominant species is that with the highest A_z value (g_z 1.940, A_z 169.0 × 10^{-4} cm^{-1}, **I**) which corresponds to *cis*-[$VO(dhp)_2(H_2O)$], together with a small amount of that with the lowest A_z (g_z 1.953, A_z 151.9 × 10^{-4} cm^{-1}, **II**) which is the isomer *trans*-[$VO(dhp)_2(H_2O)$]. No evidence of the square pyramidal [$VO(dhp)_2$] are present in the mixture H_2O/MeOH. This behavior can be explained considering that all the three species are in equilibrium, and this can be shifted by changing the media in which the spectra are recorded. Moreover, the formation of [$VO(dhp)_2$] is favored by an increase in the ionic strength, since this condition decreases the number of solvent molecules in solution "available" for metal centre coordination; on the other hand, *cis*/*trans*-[$VO(dhp)_2(H_2O)$], with a water molecule directly coordinated, are favored at low ionic strengths, when the solvent is able to coordinate the metal in the equatorial (*cis*) or axial (*trans*) position.

When the spectra are recorded in the presence of myoglobin (Fig. 1c), a new series of bands with A_z = 162.7 × 10^{-4} cm^{-1} are detected, which can be attributed to the formation of a mixed species with the composition $VO(dhp)_2$(Mb) (**IV** in Fig. 1), where an accessible His-N binds equatorially to the $VO(dhp)_2$ moiety.[26] The A_z value is intermediate to those of *cis*-[$VO(dhp)_2(H_2O)$] and [$VO(dhp)_2$] and is practically coincident with that of *cis*-[$VO(dhp)_2$(MeIm)] (163.0 × 10^{-4} cm^{-1}, **V** in Fig. 1d), which is in agreement with the literature data.[15] Probably, a small amount of binary complex remains in solution as the signals of the two isomers, *spy* and *cis-Oh*, can be noticed in the spectrum (see Fig. 1c). The experimental EPR parameters of both the binary and ternary species and the comparison with those calculated by the DFT methods are reported in Table S1.†

The EPR spectra recorded at 298 K with HEPES 0.1 M show that in the binary system only one species is present in solution and the same signals are detected in the system with 1-methylimidazole and Mb (Fig. 2). The same species was detected at temperatures higher than 298 K (Fig. S1†) and, even if the signals appear narrower, no appreciable differences were observed after the addition of MeIm to the solution. The different behavior at 298 K compared with that at 120 K can be explained by considering that only the *spy* species exists in solution at room temperature (g_0 1.976, A_0 84.1 × 10^{-4} cm^{-1}) and MeIm does not bind to V. The experimental A_0 value, measured at 298 K, was compared with that calculated from frozen solution spectrum using the relationship $A_0^{expct} = (A_x + A_y + A_z)/3$; indeed, the value obtained from the simulated spectra (Fig S2,† A_0^{expct} = 90.9 × 10^{-4} cm^{-1}) is quite different from that measured at 298 K (A_0 84.1 × 10^{-4} cm^{-1}), confirming that the mixed species *cis*-[$VO(dhp)_2$(MeIm)] is formed only at 120 K.

Moreover, at 298 K, the eventual anisotropic signals of the adduct formed by the *cis*-$VO(dhp)_2$ moiety with Mb are not detected or exist in such small amounts that cannot be revealed by EPR spectroscopy. This finding indicates that there

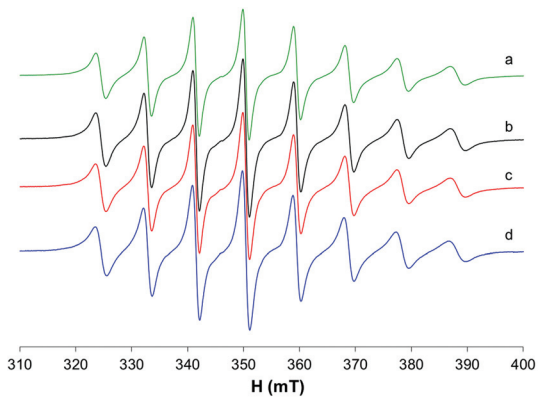

Fig. 2 Isotropic EPR spectra recorded at 298 K in solutions containing: (a) solid $VO(dhp)_2$ 1 mM dissolved in H_2O (the resulting pH is 5.90); (b) VO^{2+}/dhp 1/2, VO^{2+} 1 mM, HEPES 0.1 M, pH 7.40; (c) VO^{2+}/dhp/MeIm 1/2/4, VO^{2+} 1 mM, in HEPES 0.1 M, pH 7.40; and (d) VO^{2+}/dhp/Mb 1/2/1, VO^{2+} 1 mM, HEPES 0.1 M, pH 7.40.

is no strong covalent interaction with the protein because the only free site, that in the axial position, is not prone to the binding of the amino acid side-chains[34] and confirms that the most stable species is, at these experimental conditions, the *spy* isomer.

To evaluate if by decreasing the ionic strength it is possible to shift the equilibrium toward the formation of *cis*-[VO(dhp)$_2$(H$_2$O)], the spectrum of the binary system was also recorded without adding the HEPES buffer; as it can be noticed from Fig. 2a, no spectral changes were observed thus confirming that at 298 K the complex present in solution is [VO(dhp)$_2$].

The different behavior at 120 K can be explained considering that there is a certain percentage of the *cis* complex in solution which, in the presence of 1-methylimidazole, transforms into *cis*-[VO(dhp)$_2$(MeIm)] where the water molecule coordinated in the equatorial plane is replaced by MeIm. At the same time, the formation of this species influences the *spy* + H$_2$O ⇄ *cis-Oh* equilibrium, which is shifted toward the formation of the octahedral complex thus leading to the complete transformation into *cis*-[VO(dhp)$_2$(MeIm)] and the detection of a single signal in the EPR spectrum.

The equilibrium between the square pyramidal VO(dhp)$_2$ and the *cis*-octahedral VO(dhp)$_2$(H$_2$O) was studied by DFT calculations considering the structures of all possible isomers (Scheme S1†). The results are collected in Table S2† and it can be noticed that, both at 298 and 120 K, the values of Gibbs energy calculated for the *cis-Oh* isomers are quite close to each other with differences of less than 1 kcal mol^{-1}; therefore, it can be concluded that a mixture of the possible isomers may be present in solution. The energy of the two *spy* complexes (*SPY*-5-12 and *SPY*-5-13) is also similar.

To evaluate the influence of temperature in the *spy*/*cis-Oh* equilibrium, the ΔG_{aq} for the reaction VOL$_2$ + H$_2$O ⇄ *cis*-[VOL$_2$(H$_2$O)] has been calculated considering the corresponding average *G* values for the *spy* and *cis-Oh* forms and the contribution of the water molecule. The results suggest that the equilibrium is always shifted toward the *spy* isomer but more at 298 K where the mean value of ΔG_{aq} calculated is 10.1 kcal mol^{-1} *vs.* 5.5 kcal mol^{-1} at 120 K (see Table 1). This is in agreement with the EPR results which show that at 298 K only the [VO(dhp)$_2$] species is present in the solution, while at 120 K both square pyramidal and octahedral complexes exist, with the *spy* isomer being the predominant one.

In order to determine the most stable conformation(s) of the mixed complex *cis*-[VO(dhp)$_2$(MeIm)] at 298 and 120 K as a function of the O=V–N$_{MeIm}$–C$_{MeIm}$ dihedral angle, a series of DFT calculations were performed. Since the *G* values of the *cis-Oh* isomers are close to each other, only *OC*-6–34 and *OC*-6–23 were chosen as starting points to build the corresponding mixed complex, being the structures with the lowest and the highest energy (see Table S2†). A relaxed scan calculation was performed by changing the orientation of MeIm with respect to the V=O bond of *cis*-VO(dhp)$_2$ moiety and the results are shown in Fig. 3 and S3.† It can be noticed that the structures corresponding to the minimum points in the scan calculation are those in which the dihedral angle is 150 and 340–350°—for the *OC*-6–34 and *OC*-6–23 isomer, respectively—which were further optimized and used in the determination of G_{aq}.

The dihedral angle and Gibbs energy values calculated for the optimized structures of *cis*-[VO(dhp)$_2$(MeIm)] isomers are listed in Table S3† and their relative stability was determined considering that the starting complex can assume the *spy* geometry or the *cis-Oh* configuration. The data obtained (Table 1) suggest that the equilibrium [VO(dhp)$_2$] + MeIm ⇄ *cis*-[VO(dhp)$_2$(MeIm)] is always shifted toward the binary complex (with the positive values of ΔG_{aq} both at 298 and 120 K) in

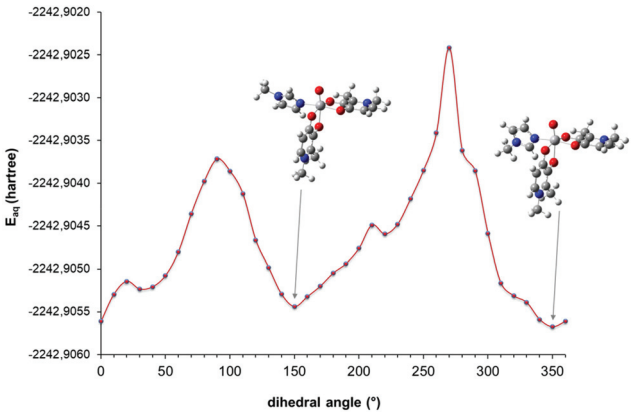

Fig. 3 Electronic energy values in solution (E_{aq}, 298.15 K) as the function of the O=V–N$_{MeIm}$–C$_{MeIm}$ dihedral angle. Relaxed scan calculation performed on the *cis*-[VO(dhp)$_2$(MeIm)] structure obtained from *OC*-6–34 isomer by substituting the water molecule with MeIm.

Table 1 ΔG values in aqueous solution for the reactions of bis-chelated VO-dhp species examined in this study[a,b]

Reaction	ΔG_{aq} (298.15 K)	ΔG_{aq} (120 K)
[VO(dhp)$_2$][c] + H$_2$O ⇄ *cis*-[VO(dhp)$_2$(H$_2$O)][d]	10.12	5.52
[VO(dhp)$_2$][c] + MeIm ⇄ *cis*-[VO(dhp)$_2$(MeIm)][e]	9.12	2.70
[VO(dhp)$_2$][c] + MeIm ⇄ *cis*-[VO(dhp)$_2$(MeIm)][f]	8.43	2.31
cis-[VO(dhp)$_2$(H$_2$O)][g] + MeIm ⇄ *cis*-[VO(dhp)$_2$(MeIm)][e] + H$_2$O	−1.69	−3.26
cis-[VO(dhp)$_2$(H$_2$O)][h] + MeIm ⇄ *cis*-[VO(dhp)$_2$(MeIm)][f] + H$_2$O	−1.34	−2.93

[a] Values reported in kcal mol^{-1}. [b] Calculations performed at the B3P86/6-311g(d,p) level of theory using the SMD model for water. [c] G_{aq} mean value of all *SPY*-5 isomers was considered. [d] G_{aq} mean value of all *OC*-6 isomers was considered. [e] G_{aq} mean value of the *OC*-6–34 isomer formed by MeIm with the two dihedral angles in Table S3† was considered. [f] G_{aq} mean value of the *OC*-6–23 isomer formed by MeIm with the two dihedral angles in Table S3† was considered. [g] G_{aq} value of the *OC*-6–34 isomer was considered. [h] G_{aq} value of the *OC*-6–23 isomer was considered.

agreement with what was observed in the EPR experiment which does not show the formation of a mixed species when only the *spy* complex is present in solution, namely at 298 K. On the other hand, when the substitution reaction *cis*-[VO(dhp)$_2$(H$_2$O)] + MeIm ⇄ *cis*-[VO(dhp)$_2$(MeIm)] + H$_2$O is taken into account, negative values of ΔG_{aq} were obtained and the results suggest that the temperature decrease favours the coordination of MeIm, as confirmed by the experimental results. The latest results explain why protein binding was detected clearly only at low temperatures.[26]

3.2. Systems with ma

The bis-chelated V^{IV}O complex formed by maltol exists in aqueous solution as a *cis*-octahedral structure [VO(ma)$_2$(H$_2$O)].[37,38,59]

The broad EPR signal obtained at 120 K (Fig. S4a†), in HEPES 0.1 M solution, suggests that different isomers can be present at physiological pH with slightly different A_z values. Among the possible geometric isomers, DFT calculations suggested that the most probable structure is that with the coordination mode [(O_{ket}, O_{phen}); (O_{ket}, O^{ax}_{phen}); H$_2$O] (Scheme S2†).[38]

In the presence of MeIm, *cis*-[VO(ma)$_2$(H$_2$O)] completely converts into the mixed complex *cis*-[VO(ma)$_2$(MeIm)] where the water molecule is replaced by the model ligand (Fig. S4c†). In the system with Mb, the EPR signal is similar to that of *cis*-[VO(ma)$_2$(MeIm)], suggesting that the species VO(ma)$_2$(Mb) is formed, with the protein coordinating the vanadium ion through an imidazole group of a histidine residue.[26]

At 298 K (Fig. 4a), when the spectra are recorded in HEPES 0.1 M, together with the predominant *cis-Oh* complex (**I**), a small amount of another species with a lower value of A_z is present in solution (whose signals are indicated with the asterisks in Fig. 4). It was noticed that at 325 and 352 K the amount of this species increases suggesting that the equilibrium depends on temperature (Fig. 4b and c). Moreover, at high temperatures the resonances are narrower, and it is possible to extract the spin Hamiltonian EPR parameters (**I** g_0 = 1.969, A_0 = 95.7 × 10^{-4} cm^{-1} and **II** g_0 = 1.974, A_0 = 84.9 × 10^{-4} cm^{-1}). The formation of species **I** was confirmed by the accordance with the experimental A_0 and that calculated from A_x, A_y and A_z measured at 120 K (Fig. S5†), where the *cis-Oh* species is the only one present in solution (A_0 = 95.7 × 10^{-4} cm^{-1} *vs.* A_0^{expct} = (A_x + A_y + A_z)/3 = 96.3 × 10^{-4} cm^{-1}).

The results are very similar to those previously obtained by Orvig and coworkers, who examined the temperature range 296–352 K.[37]

The EPR spectra were also recorded in MeOH (Fig. 5a–c); in this situation, two species are in equilibrium and their ratio changes with increasing temperature: at 335 K, the species characterized by g_0 1.974 and A_0 88.0 × 10^{-4} cm^{-1} is predominant, while at 298 K the major species is that with g_0 1.970 and A_0 96.3 × 10^{-4} cm^{-1}. In non-coordinating solvents (CHCl$_3$/toluene 6/4 v/v, Fig. 5d), only one species is observed with g_0 1.975 and A_0 90.4 × 10^{-4} cm^{-1}. Similar results were obtained by Orvig and coworkers;[37] these authors interpreted the equilibrium between different species, the square pyramidal and the two octahedral ones, *cis* and *trans*, with a solvent molecule coordinated to the metal complex. However, they were not able to distinguish between the EPR signals due to VO(ma)$_2$ and those of *trans*-VO(ma)$_2$(H$_2$O); it is now clear from the results in the literature that the effect of the solvent coordination in the axial position, *trans* to the oxido group, causes a noticeable decrease of the hyperfine coupling constant, A_0 or A_z, due to a significant decrease of the Fermi contact term.[39,43] Therefore, the two species in equilibrium in methanol solution are the *cis-Oh* and the *trans-Oh* isomers (A_0 96.3 and 88.0 × 10^{-4} cm^{-1}, **I** and **II** in Fig. 5, respectively), while the only species in non-coordinating solvents is the *spy* isomer (**III**, A_0 90.4 × 10^{-4} cm^{-1}).

In the ternary system with MeIm, small differences in the EPR spectra recorded at 298 K suggest that a small amount of the model complex *cis*-[VO(ma)$_2$(MeIm)] could be formed (Fig. 6c); this was confirmed by the results obtained at higher

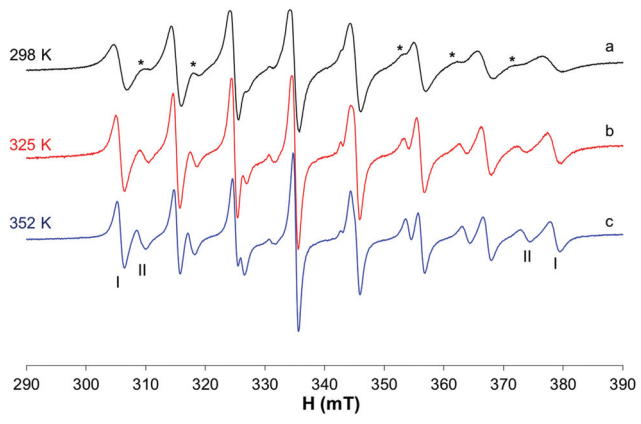

Fig. 4 Isotropic EPR spectra recorded on solutions containing VO^{2+}/ma 1/2, (VO^{2+} 1 mM, HEPES 0.1 M, pH 6.05) at variable temperatures. With **I** and **II**, the resonances of *cis*-[VO(ma)$_2$(H$_2$O)] and *trans*-[VO(ma)$_2$(H$_2$O)] are indicated.

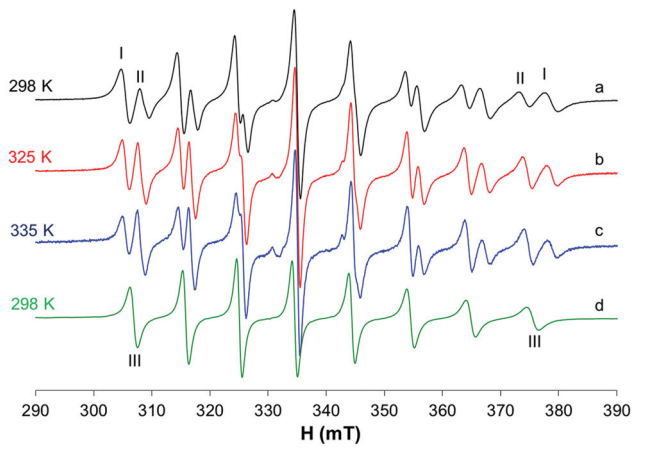

Fig. 5 Isotropic EPR spectra recorded on solutions containing solid VO(ma)$_2$ 1 mM dissolved in MeOH at variable temperatures (a–c) and (d) solid VO(ma)$_2$ 1 mM dissolved in CHCl$_3$/toluene 6/4 v/v at 298 K. With **I**, **II** and **III** the resonances of *cis*-[VO(ma)$_2$(H$_2$O)], *trans*-[VO(ma)$_2$(H$_2$O)] and [VO(ma)$_2$] are indicated.

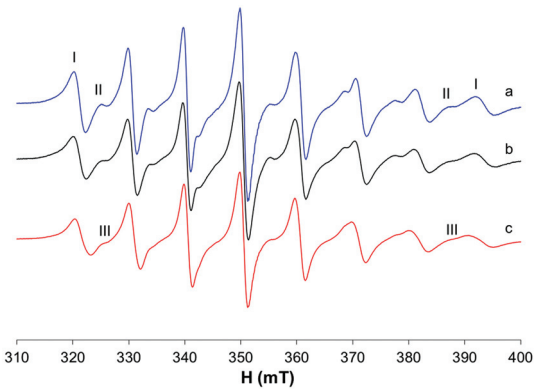

Fig. 6 Isotropic EPR spectra recorded at 298 K in solutions containing: (a) VO^{2+}/ma 1/2, VO^{2+} 1 mM, HEPES 0.1 M, pH 7.40; (b) VO^{2+}/ma/Mb 1/2/1, VO^{2+} 1 mM, HEPES 0.1 M, pH 7.40; (c) VO^{2+}/ma/MeIm 1/2/4, VO^{2+} 1 mM, HEPES 0.1 M, pH 7.40. With **I**, **II** and **III**, the resonances of *cis*-[VO(ma)$_2$(H$_2$O)], *trans*-[VO(ma)$_2$(H$_2$O)] and *cis*-[VO(ma)$_2$(MeIm)] are indicated.

temperatures (325 and 352 K) where it is possible to appreciate the presence of a new signal because of the narrowing of the bands (Fig. S6†).

On the other hand, in presence of myoglobin a similar isotropic spectrum is obtained which suggests that no binding or a very weak binding with the protein occurs (Fig. 6b).

The experimental and calculated EPR parameters of the binary and ternary species mentioned above are listed in Table S1.†

DFT calculations were performed considering four different orientations of MeIm (dihedral angle θ = 0, 90, 180, and 270°) and only the most stable *cis*-octahedral isomers where the water ligand was replaced by MeIm (Scheme S2†). The G_{aq} values at 298 and 120 K for each species are reported in Table S4† and the results of the thermodynamic calculations in Table 2. The data in Table 2 allow us to explain that the behavior of the ma complexes is probably due to the lower stability at 298 K of the mixed species. Even if the *cis-Oh* complex is formed both at 298 and 120 K — contrary to what was observed with the dhp ligand where only *spy* is present at 298 K — the calculated ΔG_{aq} values for the reaction *cis*-[VO(ma)$_2$(H$_2$O)] + MeIm ⇄ *cis*-[VO(ma)$_2$(MeIm)] + H$_2$O are more negative at 120 K (see Table 2), suggesting that the formation of the mixed complex is favored at low temperatures.

3.3. Systems with pic

The results previously published[60,61] show that in the binary system VO^{2+}/pic 1/2, vanadium is present in solution at physiological pH as a mixture of *cis*-[VO(pic)$_2$(OH)]$^-$ and

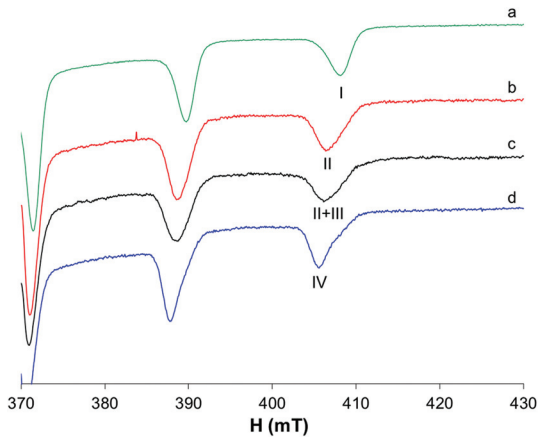

Fig. 7 Anisotropic EPR spectra recorded at 120 K in frozen solutions containing: (a) VO^{2+}/pic 1/2, VO^{2+} 1 mM, HEPES 0.1 M, pH 6.80; (b) VO^{2+}/pic 1/2, VO^{2+} 1 mM, HEPES 0.1 M, pH 7.40; (c) VO^{2+}/pic/Mb 1/2/1, VO^{2+} 1 mM, HEPES 0.1 M, pH 7.40; and (d) VO^{2+}/pic/MeIm 1/2/4, VO^{2+} 1 mM, HEPES 0.1 M, pH 7.40. With **I**, **II**, **III** and **IV**, the resonances of *cis*-[VO(pic)$_2$(H$_2$O)], *cis*-[VO(pic)$_2$(OH)]$^-$, VO(pic)$_2$(Mb), and *cis*-[VO(pic)$_2$(MeIm)] are indicated.

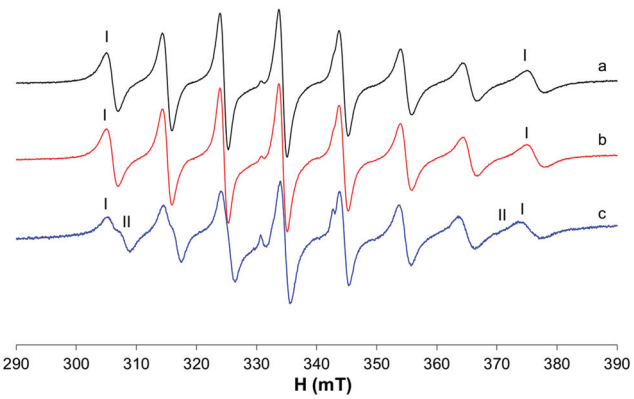

Fig. 8 Isotropic EPR spectra recorded at 298 K on solutions containing VO^{2+}/pic/Mb 1/2/1 (VO^{2+} 1 mM, HEPES 0.1 M) at different pH values: (a) 4.90, (b) 5.75 and (c) 7.55. With **I** and **II**, the resonances of *cis*-[VO(pic)$_2$(H$_2$O)] and *cis*-[VO(pic)$_2$(OH)]$^-$ are indicated.

Table 2 ΔG values in aqueous solution for the reactions of VO-ma species examined in this study[a,b]

Reaction	ΔG_{aq} (298.15 K)	ΔG_{aq} (120 K)
cis-[VO(ma)$_2$(H$_2$O)][c] + MeIm ⇄ *cis*-[VO(ma)$_2$(MeIm)][d] + H$_2$O	−1.30	−2.89
cis-[VO(ma)$_2$(H$_2$O)][e] + MeIm ⇄ *cis*-[VO(ma)$_2$(MeIm)][f] + H$_2$O	−3.79	−4.50

[a] Values reported in kcal mol^{-1}. [b] Calculations performed at the B3P86/6-311g(d,p) level of theory using the SMD model for water. [c] G_{aq} value of the *OC*-6–32 isomer was considered. [d] G_{aq} mean value of the *OC*-6–32 isomer formed by MeIm with the two dihedral angles in Table S4† was considered. [e] G_{aq} value of the *OC*-6–34 isomer was considered. [f] G_{aq} mean value of the *OC*-6–34 isomer formed by MeIm with the two dihedral angles in Table S4† was considered.

Table 3 ΔG values in aqueous solution for the reactions of VO-pic species examined in this study[a,b]

Reaction	ΔG_{aq} (298.15 K)	ΔG_{aq} (120 K)
cis-[VO(pic)$_2$(H$_2$O)][c] + MeIm ⇄ *cis*-[VO(pic)$_2$(MeIm)][d] + H$_2$O	−4.39	−5.26
cis-[VO(pic)$_2$(H$_2$O)][e] + MeIm ⇄ *cis*-[VO(pic)$_2$(MeIm)][f] + H$_2$O	−3.67	−4.86

[a] Values reported in kcal mol^{-1}. [b] Calculations performed at the B3P86/6-311g(d,p) level of theory using the SMD model for water. [c] G_{aq} value of the *OC*-6–24 isomer was considered. [d] G_{aq} mean value of the *OC*-6–24 isomer formed by MeIm with the two dihedral angles in Table S5† was considered. [e] G_{aq} value of the *OC*-6–23 isomer was considered. [f] G_{aq} mean value of the *OC*-6–23 isomer formed by MeIm with the two dihedral angles in Table S5† was considered.

cis-[VO(pic)$_2$(H$_2$O)] (Fig. 7b); the latter becomes the predominant species at lower pH (Fig. 7a) with a pK of 6.98.

To evaluate if protein coordination occurs in the system with Mb, it should be taken into account that the replacement of the equatorial OH$^-$ in *cis*-[VO(pic)$_2$(OH)]$^-$ with an imidazole nitrogen atom does not significantly change the EPR parameters, as already confirmed in the literature.[15] Therefore, even if a comparison of the spectra of the systems VO^{2+}/pic/Mb and VO^{2+}/pic at physiological pH shows very small differences (Fig. 7c), it can be supposed that an imidazole donor from Mb replaces, at least partly, the equatorial OH$^-$ ion in the hydroxido species leading to the formation of the mixed complex VO(pic)$_2$(Mb).

The differences are more visible upon comparing the resonances of the binary system with those of VO^{2+}/pic/MeIm (Fig. 7d) where, despite the similar A_z values (Table S1†), the different band shapes suggest that the coordination of MeIm to V can partially occur.

The differences are slightly visible at 298 K (Fig. S7†) also, where the neutral complex *cis*-[VO(pic)$_2$(H$_2$O)] coexists with the hydroxido species. When MeIm is added to the solution, an increase in the intensity of the internal resonances suggests that *cis*-[VO(pic)$_2$(H$_2$O)] transforms in part to *cis*-[VO(pic)$_2$(MeIm)]. The EPR spectra recorded with Mb show no clear evidence of protein binding as only isotropic signals were obtained (Fig. 8).

DFT calculations suggest that the formation of the mixed complex is thermodynamically favored since the calculated values of ΔG_{aq} for the reaction *cis*-[VO(pic)$_2$(H$_2$O)] + MeIm ⇄ *cis*-[VO(pic)$_2$(MeIm)] + H$_2$O are negative both at 298 and 120 K; as observed with the other ligands, the decrease in temperature favors the coordination of MeIm (Table 3).

4. Conclusions

In this study, the influence of different parameters, such as temperature, ionic strength, solvent and the type of ligand, on the equilibria of some oxidovanadium(IV) complexes in solution has been investigated in order to elucidate their interaction with proteins.

EPR spectroscopy is one of the most used techniques to study V^{IV}O^{2+} complexes, their equilibria and transformations in organisms after the interaction with the blood serum bioligands and cellular components. Of course, these processes take place at 37 °C (310 K) and in the liquid phase. The interaction of vanadium complexes with proteins has been mainly studied by frozen solution EPR spectroscopy (120 K) because the oxidation to V^V is minimized and anisotropic spectra can give information about the symmetry and the coordination geometry of the V^{IV}O complexes. Often, EPR studies are accompanied by UV-vis and pH-potentiometric measurements that are necessarily performed at 298 K. Therefore, in order to better analyze the results and refer them to the physiological conditions, it is important to understand how the equilibria in solution can be affected by changing the temperature and other experimental conditions.

The results of this study showed that for the potential metallodrugs VO(dhp)$_2$, VO(ma)$_2$ and VO(pic)$_2$(H$_2$O), a general equilibrium between different geometries exists in solution: VOL$_2$ + H$_2$O ⇄ *cis*-VOL$_2$(H$_2$O) ⇄ *trans*-VOL$_2$(H$_2$O). As first observed, the strength of the ligand determines the preference of penta- or hexa-coordinated structures; in particular, for the complex VO(dhp)$_2$ at 298 K only the square pyramidal species exists in aqueous solution, while the complexes VO(ma)$_2$ and VO(pic)$_2$ prefer the octahedral geometry, *cis*-VOL$_2$(H$_2$O), where the water molecule bound in the equatorial plane can deprotonate producing the corresponding mono-hydroxido species *cis*-[VOL$_2$(OH)]$^-$. This is in agreement with the data reported in the literature.[38,60] When the complex exists as *cis*-VOL$_2$(H$_2$O), the increase in temperature allows us to reveal the presence of a minor species, *trans-Oh*, due to the significant decrease in the EPR linewidth. The presence of the *trans-Oh* complex is indicated by the small value of A_0 or A_z.[39,43] It must be pointed out that the equilibria between the *spy*, *cis-Oh* and *trans-Oh* species could be more common than what is believed in the literature. They have been discussed some years ago for picolinate derivatives,[39,43] observed for dhp[39] and for maltol, even if in the latter case the authors were not able to distinguish between VO(ma)$_2$ and *trans*-[VO(ma)$_2$(H$_2$O)] species.[37]

The amount of solvent-coordinated complexes depends also on the ionic strength of the solution, which can be changed when buffers or salt are added. On the other hand, cooling the solutions down to 120 K causes the shift of the equilibria towards the octahedral species, which has been already observed with other V^{IV}O^{2+} complexes.[40,60]

When the interaction with 1-methylimidazole, a model for the side chain His coordination, was investigated, it was observed that no coordination occurs at 298 K when the V complex has a *spy* geometry, such as VO(dhp)$_2$, while the formation of the mixed species *cis*-[VOL$_2$(MeIm)] seems always to be favored by decreasing the temperature, where the com-

plexes are present as *cis*-[$VOL_2(H_2O)$] species and MeIm can easily replace the coordinated water molecule.

These effects can be related to the type of interaction observed with a protein (Mb in this study). In particular, the results obtained with all the three examined complexes provide strong evidence that the interaction with Mb is favored at low temperatures. This must be considered in the interpretation of the data. However, depending on the ligand, protein and stabilization through secondary interactions, such as hydrogen bonds and van der Waals contacts, a small amount of the adducts can also be formed at room temperature; for example, the adduct formed by *cis*-$VO(pic)_2$ with lysozyme was crystallized at 293 K and its structure is solved with the binding of Asp52-COO in one of the equatorial sites.[35]

DFT calculations permit us to evaluate the relative stability of different species in solution at different temperatures and can represent a valuable method to demonstrate this transformation, even if the stabilization of the amino acid side chains must be taken into account. The results confirm that this behavior is probably due to the lower stability at 298 K of the mixed species compared to 120 K.

Therefore, even if EPR spectra at 120 K are more easily interpretable, the lowering of the temperature can shift the equilibria and stabilize species which do not exist or exist in low amounts under physiological conditions (310 K). Therefore, EPR spectra at 298 K (or at 310 K) are surely helpful to have a more complete and realistic picture of the interaction of V complexes with proteins or other bioligands.

Considering these results, often EPR spectroscopy is not enough to characterize completely a $V^{IV}OL_2$–protein system and an integrated approach, based on the application of other techniques, such as ESI-MS, CD and ESEEM/ENDOR spectroscopy, XRD plus several computational techniques, such as docking, QM/MM and MD methods, is strongly recommended.[23,25,26,29,31,32,62]

The importance of this study is not limited to the vanadium solution chemistry since the same considerations can be extended to other metal complexes, such as Cu(II) and other first-row transition elements. Therefore, it is essential to consider the behavior of potential metallodrugs under different experimental conditions (including temperature, ionic strength, solvents, *etc.*) when their interaction with biological molecules is investigated. This fact becomes fundamental even when the results of various techniques are compared, especially when obtained under different experimental conditions.

Conflicts of interest

There are no conflicts to declare.

Acknowledgements

The authors thank Regione Autonoma della Sardegna (grant RASSR79857), Fondazione di Sardegna (grant FdS2017Garribba) and Università di Sassari (fondo di Ateneo per la ricerca 2020, Lubinu).

References

1 D. Gambino, *Coord. Chem. Rev.*, 2011, **255**, 2193–2203.
2 D. Rehder, *Future Med. Chem.*, 2012, **4**, 1823–1837.
3 J. Costa Pessoa, S. Etcheverry and D. Gambino, *Coord. Chem. Rev.*, 2015, **301–302**, 24–48.
4 D. Rehder, *Future Med. Chem.*, 2016, **8**, 325–338.
5 D. Rehder, *ChemTexts*, 2018, **4**, 20.
6 D. Crans, C. L. Yang, A. Haase and X. Yang, in *Metallo-Drugs: Development and Action of Anticancer Agents*, ed. A. Sigel, H. Sigel, E. Freisinger and R. K. O. Sigel, De Gruyter GmbH, Berlin, 2018, vol. 18, pp. 251–280.
7 S. Treviño, A. Díaz, E. Sánchez-Lara, B. L. Sanchez-Gaytan, J. M. Perez-Aguilar and E. González-Vergara, *Biol. Trace Elem. Res.*, 2019, **188**, 68–98.
8 D. C. Crans, L. Henry, G. Cardiff and B. I. Posner, in *Essential Metals in Medicine: Therapeutic Use and Toxicity of Metal Ions in the Clinic*, ed. P. L. Carver, De Gruyter GmbH, Berlin, 2019, pp. 203–230.
9 A. Ścibior, Ł. Pietrzyk, Z. Plewa and A. Skiba, *J. Trace Elem. Med. Biol.*, 2020, **61**, 126508.
10 D. Rehder, *Inorg. Chim. Acta*, 2020, **504**, 119445.
11 F. H. Nielsen, in *Handbook of Nutritionally Essential Mineral Elements*, ed. B. l. O'Dell and R. A. Sunde, Marcel Dekker, Inc., New York, 1997, ch. 22, pp. 619–360.
12 S. S. Gropper, J. L. Smith and J. L. Groff, *Advanced Nutrition and Human Metabolism*, Cengage Learning, Wadsworth, 5th edn, 2009.
13 K. H. Thompson and C. Orvig, *J. Inorg. Biochem.*, 2006, **100**, 1925–1935.
14 K. H. Thompson, J. Lichter, C. LeBel, M. C. Scaife, J. H. McNeill and C. Orvig, *J. Inorg. Biochem.*, 2009, **103**, 554–558.
15 D. Sanna, G. Micera and E. Garribba, *Inorg. Chem.*, 2010, **49**, 174–187.
16 D. Sanna, P. Buglyo, G. Micera and E. Garribba, *J. Biol. Inorg. Chem.*, 2010, **15**, 825–839.
17 D. Sanna, G. Micera and E. Garribba, *Inorg. Chem.*, 2011, **50**, 3717–3728.
18 D. Sanna, L. Bíró, P. Buglyó, G. Micera and E. Garribba, *Metallomics*, 2012, **4**, 33–36.
19 I. Correia, T. Jakusch, E. Cobbinna, S. Mehtab, I. Tomaz, N. V. Nagy, A. Rockenbauer, J. Costa Pessoa and T. Kiss, *Dalton Trans.*, 2012, **41**, 6477–6487.
20 D. Sanna, G. Micera and E. Garribba, *Inorg. Chem.*, 2013, **52**, 11975–11985.
21 J. Costa Pessoa, E. Garribba, M. F. A. Santos and T. Santos-Silva, *Coord. Chem. Rev.*, 2015, **301–302**, 49–86.
22 T. Jakusch and T. Kiss, *Coord. Chem. Rev.*, 2017, **351**, 118–126.
23 I. Correia, I. Chorna, I. Cavaco, S. Roy, M. L. Kuznetsov, N. Ribeiro, G. Justino, F. Marques, T. Santos-Silva,

M. F. A. Santos, H. M. Santos, J. L. Capelo, J. Doutch and J. Costa Pessoa, *Chem. - Asian J.*, 2017, **12**, 2062–2084.
24 D. Sanna and E. Garribba, in *An Introduction to Vanadium: Chemistry, Occurrence and Applications*, ed. R. Bowell, Nova Science Publishers, Inc., Hauppage, NY, 2019, ch. 6, pp. 141–183.
25 V. Ugone, D. Sanna, G. Sciortino, J. D. Marechal and E. Garribba, *Inorg. Chem.*, 2019, **58**, 8064–8078.
26 G. Sciortino, D. Sanna, V. Ugone, J. D. Maréchal and E. Garribba, *Inorg. Chem. Front.*, 2019, **6**, 1561–1578.
27 V. Ugone, D. Sanna, G. Sciortino, D. C. Crans and E. Garribba, *Inorg. Chem.*, 2020, **59**, 9739–9755.
28 G. Sciortino and E. Garribba, *Chem. Commun.*, 2020, **56**, 12218–12221.
29 A. Banerjee, S. P. Dash, M. Mohanty, G. Sahu, G. Sciortino, E. Garribba, M. F. N. N. Carvalho, F. Marques, J. Costa Pessoa, W. Kaminsky, K. Brzezinski and R. Dinda, *Inorg. Chem.*, 2020, **59**, 14042–14057.
30 A. Levina and P. A. Lay, *Inorg. Chem.*, 2020, **59**, 16143–16153.
31 V. Ugone, D. Sanna, S. Ruggiu, G. Sciortino and E. Garribba, *Inorg. Chem. Front.*, 2021, **8**, 1189–1196.
32 J. Costa Pessoa, M. F. A. Santos, I. Correia, D. Sanna, G. Sciortino and E. Garribba, *Coord. Chem. Rev.*, 2021, **449**, 214192.
33 E. Garribba, G. Micera and D. Sanna, *Inorg. Chim. Acta*, 2006, **359**, 4470–4476.
34 G. Sciortino, V. Ugone, D. Sanna, G. Lubinu, S. Ruggiu, J.-D. Maréchal and E. Garribba, *Front. Chem.*, 2020, **8**, 345.
35 M. F. A. Santos, I. Correia, A. R. Oliveira, E. Garribba, J. Costa Pessoa and T. Santos-Silva, *Eur. J. Inorg. Chem.*, 2014, 3293–3297.
36 G. Sciortino, D. Sanna, V. Ugone, G. Micera, A. Lledós, J.-D. Maréchal and E. Garribba, *Inorg. Chem.*, 2017, **56**, 12938–12951.
37 G. R. Hanson, Y. Sun and C. Orvig, *Inorg. Chem.*, 1996, **35**, 6507–6512.
38 D. Sanna, P. Buglyó, L. Bíró, G. Micera and E. Garribba, *Eur. J. Inorg. Chem.*, 2012, 1079–1092.
39 S. Gorelsky, G. Micera and E. Garribba, *Chem. – Eur. J.*, 2010, **16**, 8167–8180.
40 D. Sanna, V. Ugone, G. Micera and E. Garribba, *Dalton Trans.*, 2012, **41**, 7304–7318.
41 P. Buglyó, T. Kiss, E. Kiss, D. Sanna, E. Garribba and G. Micera, *J. Chem. Soc., Dalton Trans.*, 2002, 2275–2282.
42 C. Orvig, P. Caravan, L. Gelmini, N. Glover, F. G. Herring, H. Li, J. H. McNeill, S. J. Rettig and I. A. Setyawati, *J. Am. Chem. Soc.*, 1995, **117**, 12759–12770.
43 E. Lodyga-Chruscinska, G. Micera and E. Garribba, *Inorg. Chem.*, 2011, **50**, 883–899.
44 D. Sanna, E. Garribba and G. Micera, *J. Inorg. Biochem.*, 2009, **103**, 648–655.
45 M. J. Frisch, G. W. Trucks, H. B. Schlegel, G. E. Scuseria, M. A. Robb, J. R. Cheeseman, G. Scalmani, V. Barone, B. Mennucci, G. A. Petersson, H. Nakatsuji, M. L. Caricato, X. H. P. Hratchian, A. F. Izmaylov, J. Bloino, G. Zheng, J. L. Sonnenberg, M. Hada, M. Ehara, K. Toyota, R. Fukuda, J. Hasegawa, M. Ishida, T. Nakajima, Y. Honda, O. Kitao, H. Nakai, T. Vreven, J. A. Montgomery Jr., J. E. Peralta, F. Ogliaro, M. Bearpark, J. J. Heyd, E. Brothers, K. N. Kudin, V. N. Staroverov, T. Keith, R. Kobayashi, J. Normand, K. Raghavachari, A. Rendell, J. C. Burant, S. S. Iyengar, J. Tomasi, M. Cossi, N. Rega, J. M. Millam, M. Klene, J. E. Knox, J. B. Cross, V. Bakken, C. J. Adamo, J. R. Gomperts, R. E. Stratmann, O. Yazyev, A. J. Austin, R. Cammi, C. Pomelli, J. W. Ochterski, R. L. Martin, K. Morokuma, V. G. Zakrzewski, G. A. Voth, P. Salvador, J. J. Dannenberg, S. Dapprich, A. D. Daniels, Ö. Farkas, J. B. Foresman, J. V. Ortiz, J. Cioslowski and D. J. Fox, *Gaussian 09, revision C.01*, Gaussian, Inc., Wallingford, CT, 2010.
46 M. Bühl and H. Kabrede, *J. Chem. Theory Comput.*, 2006, **2**, 1282–1290.
47 M. Bühl, C. Reimann, D. A. Pantazis, T. Bredow and F. Neese, *J. Chem. Theory Comput.*, 2008, **4**, 1449–1459.
48 G. Micera and E. Garribba, *Int. J. Quantum Chem.*, 2012, **112**, 2486–2498.
49 A. V. Marenich, C. J. Cramer and D. G. Truhlar, *J. Phys. Chem. B*, 2009, **113**, 6378–6396.
50 G. Micera, V. L. Pecoraro and E. Garribba, *Inorg. Chem.*, 2009, **48**, 5790–5796.
51 D. Sanna, K. Varnágy, S. Timári, G. Micera and E. Garribba, *Inorg. Chem.*, 2011, **50**, 10328–10341.
52 G. Micera and E. Garribba, *Eur. J. Inorg. Chem.*, 2011, **2011**, 3768–3780.
53 D. Sanna, V. L. Pecoraro, G. Micera and E. Garribba, *J. Biol. Inorg. Chem.*, 2012, **17**, 773–790.
54 S. Kundu, D. Mondal, K. Bhattacharya, A. Endo, D. Sanna, E. Garribba and M. Chaudhury, *Inorg. Chem.*, 2015, **54**, 6203–6215.
55 S. P. Dash, S. Majumder, A. Banerjee, M. F. N. N. Carvalho, P. Adão, J. Costa Pessoa, K. Brzezinski, E. Garribba, H. Reuter and R. Dinda, *Inorg. Chem.*, 2016, **55**, 1165–1182.
56 G. Micera and E. Garribba, *Dalton Trans.*, 2009, 1914–1918.
57 G. Micera and E. Garribba, *J. Comput. Chem.*, 2011, **32**, 2822–2835.
58 D. Sanna, G. Sciortino, V. Ugone, G. Micera and E. Garribba, *Inorg. Chem.*, 2016, **55**, 7373–7387.
59 D. Sanna, L. Bíró, P. Buglyó, G. Micera and E. Garribba, *J. Inorg. Biochem.*, 2012, **115**, 87–99.
60 E. Kiss, E. Garribba, G. Micera, T. Kiss and H. Sakurai, *J. Inorg. Biochem.*, 2000, **78**, 97–108.
61 E. Kiss, K. Petrohán, D. Sanna, E. Garribba, G. Micera and T. Kiss, *Polyhedron*, 2000, **19**, 55–61.
62 G. Sciortino, J. D. Maréchal and E. Garribba, *Inorg. Chem. Front.*, 2021, **8**, 1951–1974.